Bioactive Materials 14 (2022) 350–363

Contents lists available at ScienceDirect

Bioactive Materials

journal homepage: www.keaipublishing.com/en/journals/bioactive-materials

Decoding the annulus fibrosus cell atlas by scRNA-seq to develop an inducible composite hydrogel: A novel strategy for disc reconstruction

Han Wang [a,b,1], Di Wang [a,1], Beier Luo [c,1], Dong Wang [a], Haoruo Jia [a], Pandi Peng [a], Qiliang Shang [a], Jianxin Mao [a], Chu Gao [a], Ye Peng [b], Lu Gan [b], Junjie Du [b], Zhuojing Luo [a,d,**], Liu Yang [a,d,*]

[a] Department of Orthopedics, Xijing Hospital, Fourth Military Medical University, Xi'an, 710032, China
[b] Department of Orthopedics, Air Force Medical Center, 100142, Beijing, China
[c] Department of Spinal Surgery, Changhai Hospital, Naval Medical University, Shanghai, 200433, China
[d] Medical Research Institute, Northwestern Polytechnical University, Xi'an, 710072, China

ARTICLE INFO

Keywords:
Single cell RNA-Seq
Annulus fibrosus-derived stem cells
Lineage tracing
Composite hydrogel
Annulus fibrosus reconstruction

ABSTRACT

Low back pain is one of the most serious public health problems worldwide and the major clinical manifestation of intervertebral disc degeneration (IVDD). The key pathological change during IVDD is dysfunction of the annulus fibrosus (AF). However, due to the lack of an in-depth understanding of AF biology, the methods to reconstruct the AF are very limited. In this study, the mice AF cell atlas were decoded by single-cell RNA sequencing to provide a guide for AF reconstruction. The results first identify a new population of AF cells, fibrochondrocyte-like AF cells, which synthesize both collagen I and collagen II and are potential functional cells for AF reconstruction. According to the dual features of the AF extracellular matrix, a composite hydrogel based on the acylation of methacrylated silk fibroin with methacrylated hyaluronic acid was produced. To obtain the ability to stimulate differentiation, the composite hydrogels were combined with a fibrochondrocyte-inducing supplement. Finally, reconstruction of the AF defects, by the novel AF stem cell-loaded composite hydrogel, could be observed, its amount of chondroid matrices recovered to 31.7% of AF aera which is significantly higher than that in other control groups. In summary, this study decodes the AF cell atlas, based on which a novel strategy for AF reconstruction is proposed.

1. Introduction

Low back pain is a public health problem with high morbidity, of which the combined lifetime prevalence can reach approximately 47% in many countries [1]. The main cause of low back pain is intervertebral disc degeneration (IVDD), which also leads to skin paresthesia, muscle paralysis, and even paraplegia in patients, seriously affecting their quality of life [2,3]. Annulus fibrosus (AF) defects are the key pathological changes during IVDD, which directly cause herniation of the nucleus pulposus (NP) and subsequently lead to the release of inflammatory factors and compression of the nerve root and spinal cord. Therefore, reconstructing AF defects is the key problem when treating IVDD [4].

To date, there is a lack of satisfying clinical methods for AF repair. Surgical suturing is one such method to repair AF injury. However, the natural repair process of the sutured AF mainly occurs by scar healing, which is a potential risk for injury recurrence because of changes in the local mechanical properties [5]. In addition, the direct suturing of AF defects of a certain scale would cause considerable tension, which would delay healing and produce a larger amount of scar tissue [6–8]. In addition to sutures, annular closure devices (ACDs) have been recently developed and applied in the clinic to block off the AF defect [9]. However, because the shapes of ACDs are immutable, they are not suitable for use in large or irregularly shaped AF defects. In addition, with limited biocompatibility, biological fusion between the ACDs and AF is difficult, which affects its long-term therapeutic effects [9–11].

Peer review under responsibility of KeAi Communications Co., Ltd.
* Corresponding author. Department of Orthopedics, Xijing Hospital, Fourth Military Medical University, 710032, Xi'an, China.
** Corresponding author. Department of Orthopedics, Xijing Hospital, Fourth Military Medical University, 710032, Xi'an, China.
E-mail addresses: zjluo@fmmu.edu.cn (Z. Luo), yangliu@fmmu.edu.cn (L. Yang).
[1] These authors contributed equally to this work.

https://doi.org/10.1016/j.bioactmat.2022.01.040
Received 7 November 2021; Received in revised form 22 January 2022; Accepted 23 January 2022
Available online 3 February 2022

To improve upon the above drawbacks, tissue engineering techniques have shown promise for AF repair. Previous studies have used natural biomaterials, such as high-density collagen gel or fibrin gel, to reconstruct AF defects, which have the advantage of high biocompatibility and the disadvantage of low stretching resistance [12–14]. Synthesized polymer materials, such as polyglycolic acid/polyvinylidene fluoride (PAPF) and poly lactic-co-glycolic acid (PLGA), have been used to reconstruct AF defects to increase mechanical strength at the expense of biocompatibility [15,16]. In recent years, a tissue engineering strategy combining both seeding cells and diverse scaffolds has been applied to the reconstruction of the AF. AF-derived stem cells are the multipotent stem cells obtained from AF tissue, which are eligible seed cells for AF repair because of the closest relatives [17]. In addition, as they are convenient to obtain and readily proliferate, mesenchymal stem cells (MSCs) have also been used for AF repair. Both AFSCs cell-laden decellularized matrix/chitosan hydrogels [18] and MSC-laden cross-linked high-density collagen gels [19] were suggested to be more effective than acellular biomaterials for AF reconstruction.

Even so, there are still some problems waiting to be solved in terms of AF reconstruction with cells and biomaterials. Cell-laden or acellular materials mostly restore fibrous tissue in the outer AF (oAF) with little restoration in the chondroid components of the inner AF (iAF) [13,15,19–21]. There are several reasons for these results. First, AF cells are heterogeneous, and restoring multiple types of AF cells and extracellular matrix by using a single kind of seed cell and a single inductive environment is difficult [22]. In addition, the local microenvironment of the areas being repaired *in vivo* affects the expected differentiation of seed cells, making it uncontrollable. Therefore, developing a novel inductive biomaterial to match the multiple types of AF cells and matrix is essential for AF reconstruction.

To resolve the above problems, the following research gaps need to be filled. First, the heterogeneity of AF cells should be fully understood to establish the targets of the induction strategy. In addition, a composite hydrogel with inductive activity should be designed and constructed to adapt to a variety of AF cell and matrix types. Therefore, in this study, we aimed to use single-cell RNA sequencing (scRNA-seq) technology to decode the AF cell atlas, provide a guide for AF reconstruction, explore an inductive composite hydrogel, and finally test its reparative effects in an AF defect model *in vivo*. In this way, we can propose a novel strategy for AF reconstruction to advance the therapeutic methods for AF injury and IVDD (Scheme 1).

2. Experimental section

2.1. Single-cell RNA sequencing

Isolation of single cells: All animal experiments were performed in accordance with a protocol approved by the Institutional Animal Care and Use Committee of AFMU. Primary AF tissues were collected from C57BL/6J mice at the ages of postnatal 1 and 10 months (P1 M and P10 M). The time from AF sample collection to processing was 30 min or less. Single-cell suspensions of AF tissues were obtained by mechanical dissociation and enzymatic digestion, and the resulting cell suspensions were filtered through a 40 μm nylon cell strainer. Dead cells were removed with a Dead Cell Removal Kit (Miltenyi Biotec), and the cell survival rate was generally above 99%. A total of 50000 cells were loaded onto an individual 10–17 mm integrated fluidic circuit mRNA sequencing chip in a C1 Single-Cell Auto Prep System (Fluidigm), and the loaded chips were microscopically examined to verify single-cell loading.

2.2. cDNA amplification

For cell lysis and cDNA synthesis and amplification, a SMARTer Ultra Low RNA Kit (Clontech) was used following the manufacturer's instructions. RNA spike-ins 1, 4, and 7 (ArrayControl RNA Spikes, Thermo Fisher) were added to the lysis mix. The quantity and quality of the amplified cDNAs were measured using a Qubit 2.0 fluorometer (Life Technologies) and 2100 Bioanalyzer (Agilent Technologies), respectively.

2.3. Droplet-based scRNA-seq

scRNA-seq was performed at Genergy Bio (Shanghai, China). In total,

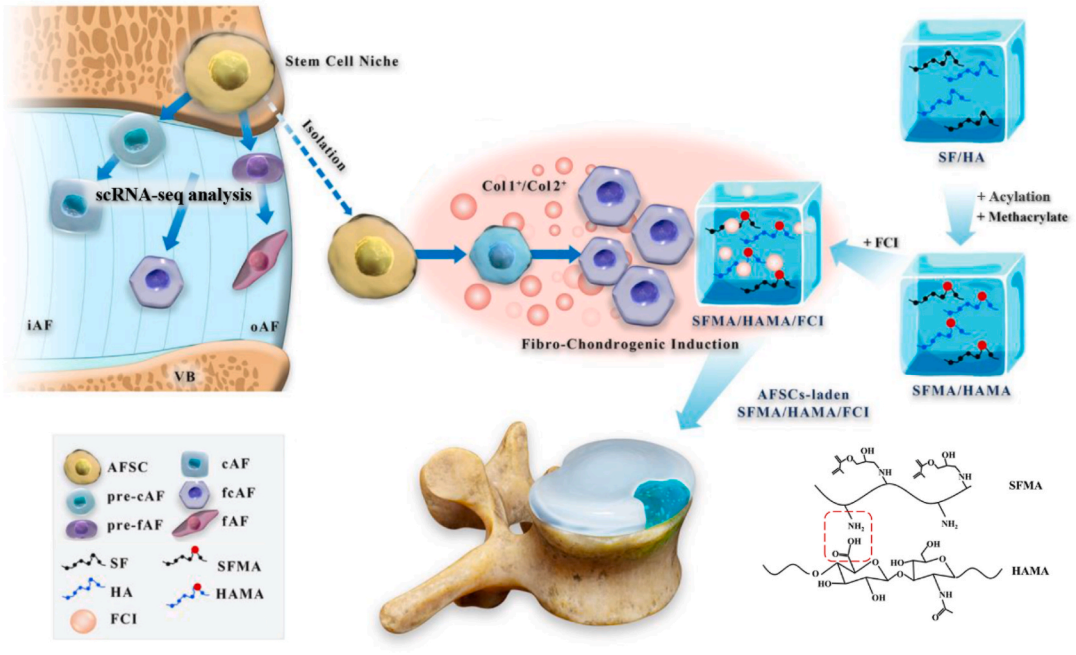

Scheme 1. Schematic illustration of A novel strategy for disc reconstruction based on single-cell RNA sequencing and composite hydrogel. VB, vertebra bone; iAF, inner AF; oAF, outer AF; AFSC, AF stem cells; cAF, chondrocyte-like AF cells; fAF, fibroblast-like AF cells; SF, silk fibroin; HA, hyaluronic acid; MA, methacrylate; FCI, fibrochondrocyte-inducing supplement.

3000 single-cell cDNAs were subjected to RNA sequencing. Briefly, single-cell suspensions were converted into barcoded scRNA-seq libraries by using a Chromium Single Cell 3′ Reagent Kit v2 (10 × Genomics). Libraries were sequenced on an Illumina HiSeq4000. Data were analyzed and mapped to the mouse genome (mm10) using CellRanger software (10 × Genomics) [23].

2.4. Isolation and culture of mouse AFSCs

AFSCs were isolated from C57BL/6J mouse (2–4 weeks old) AF tissue and cultured in DMEM F12 1:1 (HyClone) supplemented with 10% fetal bovine serum (FBS; HyClone) as described previously [24]. Briefly, we harvested mouse spinal columns from T10 to L5 and C2–C8 in a sterile environment and carefully removed the surrounding muscles and ligaments. Then, the spinal column of each IVD was transversally sectioned. After carefully removing the NP, the pure AF tissue was minced and digested in DMEM with collagenase P (1 mg/mL) for 2–4 h. The obtained suspension was then centrifuged at 1000 rpm for 5 min, and then the cell pellet was resuspended in DMEM containing 10% FBS, 100 U/mL penicillin, and 100 μg/mL streptomycin and maintained in a humidified incubator at 37 °C with 5% CO_2 at a density of 200–500 cells/mL. The culture medium was changed every 2 days until the cells became subconfluent. The cells were then harvested using 0.25% trypsin-EDTA. In our research, we used third to fifth passage AFSCs.

2.5. Animals and treatments

We purchased LepR-Cre mice (stock no. 008320), R26R-TdTomato mice (stock no. 007909) from the Jackson Laboratory (Bar Harbor, ME, USA). Male C57BL/6 mice of all ages were obtained from the Experimental Animal Center of the Fourth Military Medical University and housed in cages at 22 °C on a 12 h light/dark cycle. All animal procedures were performed with the approval by Institutional Animal Care and Use Committee (IACUC) of Fourth Military Medical University (No. 20200526).

Mice (P1M) were divided into six groups of six mice each as follows: baseline (BL) group, control (Con) group, AF injured group, SFMA/HAMA group, SFMA/HAMA + Cell group, and SFMA/HAMA/FCI + Cell group. The mice in the BL group were sampled before the start of the experiment to determine the baseline conditions. The control group was defined as those without AF injury, and the AF injured group was defined as those subjected to only AF injury and repair by treatment with normal saline. The other three groups underwent surgical transplantation with the corresponding composite hydrogels after induced AF injury. Surgery was performed under general anesthesia using 2.5% isoflurane inhalation while in the prone position. The base of the tail was avascularized using rubber bands. The tail IVDs Cy 5/6, 6/7, and 7/8 were exposed in each animal. A 0.8 × 0.5 mm defect, approximately 0.4 mm deep (without releasing the NP tissue), was generated on each mouse using a microscope. Subsequently, for the repair groups, the appropriate composite hydrogels were directly dropped into the AF defects and cured by irradiation with 405 nm light. Then, after 2 months of modeling, the mice were euthanized and sampled.

2.6. Preparation of the FCI

Fibrochondrogenic inductive medium was used to induce AFSC differentiation into fcAFs. After the formulation and dosage were explored in preliminary experiments *in vitro*, the composition of inductive medium we finally used in this study was 10% FBS, 10 mM β-glycerophosphate, 10 ng/mL TGF-β3, 37.5 μg/mL ascorbic acid, and 0.1 μM dexamethasone in DMEM.

2.7. Synthesis of SFMA

Methacrylated SF (SFMA) was synthesized as described previously [25]. Briefly, 40 g of silkworm cocoon was boiled in 2 L of 2% Na_2CO_3 solution for 30 min at 100 °C and then washed several times with distilled water. Subsequently, the degummed silk was dried in an oven at 40 °C, and 424 mM glycidyl methacrylate (GMA) solution was added at a rate of 0.5 mL/min to a 20% (w/v) solution of SF in 9.3 M lithium bromide (LiBr) under constant stirring for 3 h at 60 °C. After the reaction, the resultant polymer solution was dialyzed against distilled water for 4 days. Finally, the freeze-dried SFMA samples were stored at −80 °C for further use.

2.8. Synthesis of HAMA

Methacrylation of HA was performed by the dropwise addition of 1.1 mL of 1% (v/v) MA to 100 mL of a 1% (w/v) HA solution in PBS pH 7.4, at 4 °C under magnetic stirring for 24 h. The pH of the solution was maintained between 8 and 10 with the addition of 5 M NaOH until no further pH changes were detected, which indicated that the reaction was complete. The solution was dialyzed for 4 days in a 12–14 kDa membrane in deionized water at 4 °C. HAMA was frozen in liquid nitrogen and lyophilized, and the obtained powder material was stored at −20 °C until further use [26].

2.9. Preparation of the SFMA/HAMA/FCI

After the preliminary experiment to optimize hydrogel concentration, we finally determined that the SFMA/HAMA composite hydrogel should be formed by mixing 4% (w/v) SFMA and 2% (w/v) HAMA. The mixture was heated in 65 °C waterbath for 30 min to accelerate the dissolution and acylation. Then, 10 mM B-glycerophosphate, 10 ng/mL TGF-β3, 50 μg/mL ascorbic acid, and 0.1 mM dexamethasone were added to the SFMA/HAMA composite hydrogel. The composite hydrogels were mixed with a photoinitiator (0.25% lithium phenyl (2,4,6-trimethylbenzoyl) phosphinate (LAP)) and stored shielded from light [27].

2.10. Statistical analysis

The experimental data were statistically analyzed with the SPSS 19.0 software. The data were expressed as the mean ± SD of at least three independent experiments *in vitro* and six independent experiments *in vivo*. Comparisons of normally distributed data between two independent groups were performed using a two-tailed *t*-test. One-way analysis of variance (ANOVA) followed by Dunnett's test was conducted to test the normally distributed continuous variable from more than two independent groups. Comparisons of discontinuous variable data, histological scores, used Kruskal-Wallis h-test followed by Dunn's multiple comparisons tests. A *P* value of less than 0.05 was considered significant.

3. Results

3.1. Single-cell RNA sequencing of mouse AF cells reveals 10 populations

To gain greater insights into the heterogeneity of AF cells, we performed scRNA-seq on AF tissues from P1 M and P10 M mice. In total, we sequenced 3555 individual AF cells for subsequent analysis after rigorous filtration. We charted the microenvironment landscape in the AF cells of mice with t-distributed stochastic neighbor embedding (t-SNE) plots (Fig. 1a). Based on our comprehensive analysis, we identified 10 major cell populations: AF stem cells (AFSCs), chondrocyte-like AF progenitor cells (cAF progenitors), fibroblast-like AF progenitor cells (fAF progenitors), prechondrocyte-like AF cells (pre-cAFs), prefibroblast-like AF cells (pre-fAFs), immature chondrocyte-like AF cells (immature cAFs), immature fibroblast-like AF cells (immature fAFs), mature chondrocyte-like AF cells (mature cAFs), mature fibroblast-like AF cells (mature fAFs), and fibrochondrocyte-like AF cells (fcAFs). The differentially expressed genes (DEGs) that defined each

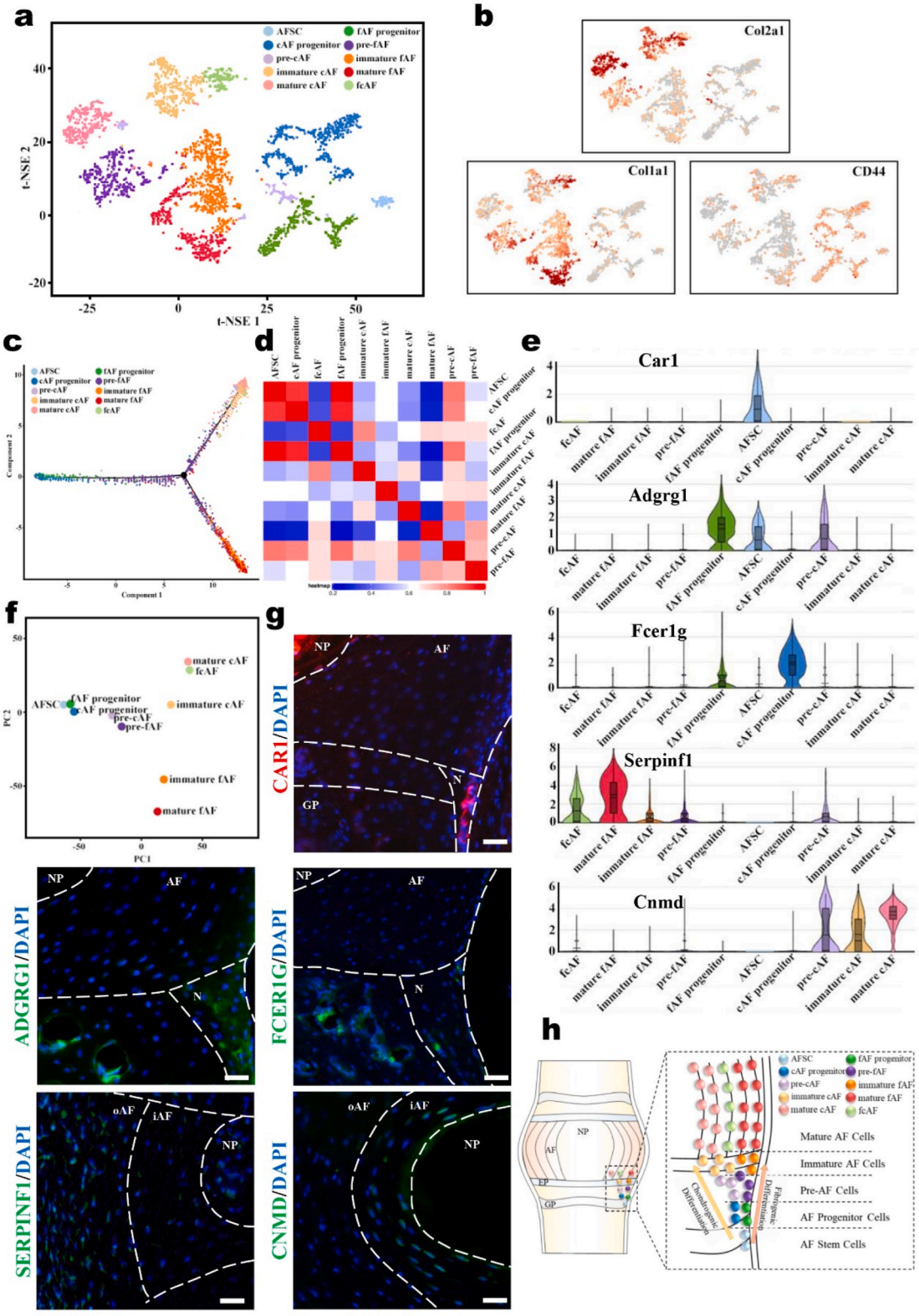

Fig. 1. scRNA-seq reveals 10 major cell populations in the murine AF. (a) Visualization of the t-SNE plots colored according to cell populations for mouse AF cell single-cell transcriptomes. (b) Dot plots showing the expression of the indicated markers for the populations on the t-SNE map. (c) Pseudo-time trajectory analysis revealing AF cell lineage progression colored according to cell population. (d) Heatmap showing the pairwise correlations of AF populations. (e) Violin plots showing the expression levels of representative candidate marker genes for the five main AF populations. (f) PCA visualization showing the affinity-disaffinity relationship among AF populations. (g) Representative immunofluorescence assay of the indicated marker genes in IVD tissues. Scale bars, 50 μm. (h) Schematic diagram of the 10 AF populations in the IVDs.

population are presented in the Supporting Information (Supplementary Fig. 1). the distribution of the representative markers CD44, Col1a1 and Col2a1 in the t-SNE map showed that the AF cells were divided into three main categories: progenitor cells, fibroblast-like cells, and chondrocyte-like cells (Fig. 1b). Further pseudo-time analysis revealed their differentiation relationship, and the AF cells were arranged into three major clades that indicated the two directions of differentiation from progenitor cells: fibrogenic differentiation and chondrogenic differentiation (Fig. 1c). Furthermore, pairwise correlation analysis and principal component analysis (PCA) (Fig. 1d and e) revealed close relationships among the AFSCs, fAF progenitors and cAF progenitors as well as the pre-fAFs and pre-cAFs. With continued differentiation, the relationships became somewhat distant among immature fAFs, immature cAFs, mature fAFs and mature fAFs**.** By analyzing the molecular signatures of these populations with scRNA-seq, we found that the genes Car1, Adgrg1, Fcer1g, Serpinf1 and Cnmd were specifically highly expressed in AFSCs, fAF progenitors, cAF progenitors, mature fAFs and mature cAFs, respectively (Fig. 1f). We then performed an immunofluorescence assay to validate these markers for the five main populations and detected their locations *in vivo* (Fig. 1g). The results revealed that AFSCs, fAF progenitors and cAF progenitors were distributed in the area adjacent to the epiphyseal plate, which has been defined as the stem cell niche of the intervertebral disc (IVD). Mature fAFs and mature cAFs were distributed in the oAF and iAF, respectively. Therefore, our data revealed that AFSCs are located in IVD niches and begin to differentiate into one of two directions, fibrogenic or chondrogenic, at the beginning of migration. Along with the following migration process, the AFSCs gradually go through three cell stages: progenitor cells, pre-AF cells and immature AF cells, finally differentiating into mature fAFs and cAFs (Fig. 1h). Our study decodes the AF cell atlas, providing a cytological basis for AF biology.

3.2. AFSCs are eligible cells for AF reconstruction with the potential to differentiate into AF cells

By analyzing the scRNA-seq data, we found specific marker genes of AFSCs, including CD69, CD105, Gata2 and Tnfaip3 (Fig. 2a). Immunofluorescence staining of GATA2 further verified the scRNA-seq data and confirmed that the AFSCs were located in IVD niches (Fig. 2b). To investigate the differentiation of AFSCs under normal physiological conditions, we discovered that CD63 and Bgn gradually became upregulated in the process from AFSCs to mature fAFs; similarly, CD24a and Higd1a were upregulated in the process from AFSCs to mature cAFs. These data indicated that these genes were related to AFSC differentiation.

On the other hand, as CD105 is a marker of AFSCs and we found that the majority of $CD105^+$ cells were leptin receptor (LepR)-positive cells (Fig. 2d), we used $LepR^+$ cells to represent AFSCs and investigated their migration by tracing $LepR^+$ lineage cells using genetic labeling. LepR has been reported as an important marker of bone marrow mesenchymal stem cells (BMSCs) and labels the progenitor subpopulation, which subsequently differentiates into both osteoblasts and adipocytes [28,29]. We crossed LepR-Cre mice with R26R-tdTomato mice to generate LepR-Cre; R26R-tdTomato mice and then traced the $tdTomato^+$ cells in the IVD. We confirmed the colocalization of the CD105 and LepR-tdTomato signals by immunostaining (Fig. 2e). Moreover, we observed the migration route of $tdTomato^+$ cells in both the niche and AF area in P2W LepR-Cre; tdTomato mice (Fig. 2f). Over time, the $tdTomato^+$ cells migrated into the AF area from the IVD niches and gradually diffused throughout the AF. At the age of P10 M, the proportion of $tdTomato^+$ cells in the AF was approximately 42.8% (Fig. 2f and Supplementary Fig. 2). The three-dimensional perspective of the IVD further demonstrated that the $tdTomato^+$ cells were distributed uniformly in the AF of adult mice (Fig. 2g). Aside from the AF area, we noticed that $tdTomato^+$ cells were also located in the NP, which is consistent with our previous report [30]. To verify the migration of this population, we established distinct AF damage models interrupting either the AF migration route or niche at P2W, with sampling and observation at P6W. In the migration route damage model, we found that the number of $tdTomato^+$ cells was reduced to almost zero after eliminating the migration route (Fig. 2h). In the niche damage model, the number of $tdTomato^+$ cells was also reduced to almost zero after thermal ablation of the niches (Fig. 2j). Thus, for the first time, our study identified the migration of AFSCs by lineage tracing.

To further explore the possibility of culturing AFSCs *in vitro* to provide a better strategy for AF construction, primary AFSCs were isolated and purified from the IVDs of P1M mice. The cultured AFSCs were fusiform or polygonal as previously reported [17,31,32] (Fig. 2i). Flow cytometric analysis showed that the primary AFSCs highly expressed the stem cell markers CD90 and CD105 but did not express the hematopoietic markers CD34 and CD45 (Fig. 2l), which is consistent with previous reports [33]. Further immunofluorescence assays showed that the cultured AFSCs expressed GATA2, which is consistent with our scRNA-seq results (Fig. 2k). These data demonstrated that the AFSCs located in the IVD niches can migrate and differentiate into AF cells and might be appropriate for AF reconstruction.

3.3. A novel AF population expressing typical molecular markers of both the iAF and oAF was identified

By analyzing the scRNA-seq data, we found that fcAFs combined the features of both fAFs and cAFs. fcAFs expressed not only fibrogenic markers, such as Col1a1, Col1a2, and Serpinf1, but also chondrogenic markers, such as Col2a1, Acan, and Sox9 (Fig. 3a). Further immunofluorescence analysis showed that COLI and COLII were colocalized in the middle layers of AF tissue, indicating that these cells could produce and synthesize both COLI and COLII (Fig. 3b and c). These populations were consistently found in the AF of both newborn and adult mice (Fig. 3e). After further exploration, we found specific molecular markers of fcAFs by scRNA-seq, including Igfbp6 and Tnxb (Fig. 3e and Supplementary Fig. 3). By immunofluorescence, these two markers were verified to be specifically located in the middle layers of AF tissue (Fig. 3f, h). According to the above results, we first identified a novel cell type, fcAFs, that existed in the middle layers of AF and appeared to have characteristics of both fibroblast-like and chondrocyte-like AF cells. Additionally, KEGG analysis showed that focal adhesion and ECM-receptor interaction signaling pathways were enriched in fcAFs, which strongly correlate with important biological processes, including cell motility, differentiation, and survival (Fig. 3g). We then compared the differences between fcAFs and fAFs/cAFs and found that the TGF-β, PI3K-AKT and glycan biosynthesis signaling pathways were highly expressed in fcAFs (Fig. 3i and Supplementary Fig. 4), indicating that fcAFs are a population of cells with high metabolic activity in AF tissue. Therefore, it is promising to use fcAFs as the seed cell induction target to repair AF injury through tissue engineering based on its high activity and the ability to synthesize the matrix of both the oAF and iAF.

3.4. AFSCs were induced and differentiated into fcAFs in vitro

Determining how to enhance the inductive ability and control the differentiation process of seed cells are critical problems in AF reconstruction strategies. To enhance the directed induction ability of the biomaterial scaffold, we designed a fibrochondrogenic inductive supplement (FCI), which consisted of β-glycerophosphate, TGF-β3, ascorbic acid, and dexamethasone. To examine the inductive effects of the FCI, AFSCs were cultured in medium with FCI for 2 weeks. The expression levels of the fibrogenic markers Col1a1, Scx, Sp7, Bglap and Tnmd, which were reported previously [34–36], were upregulated in fibrogenic or fibrochondrogenic medium but not in chondrogenic medium (Fig. 4a). Moreover, the expression levels of the chondrogenic markers Col2a1, Acan, Sox9, Prg4 and Cnmd, which were reported previously [37,38], were upregulated in chondrogenic or fibrochondrogenic

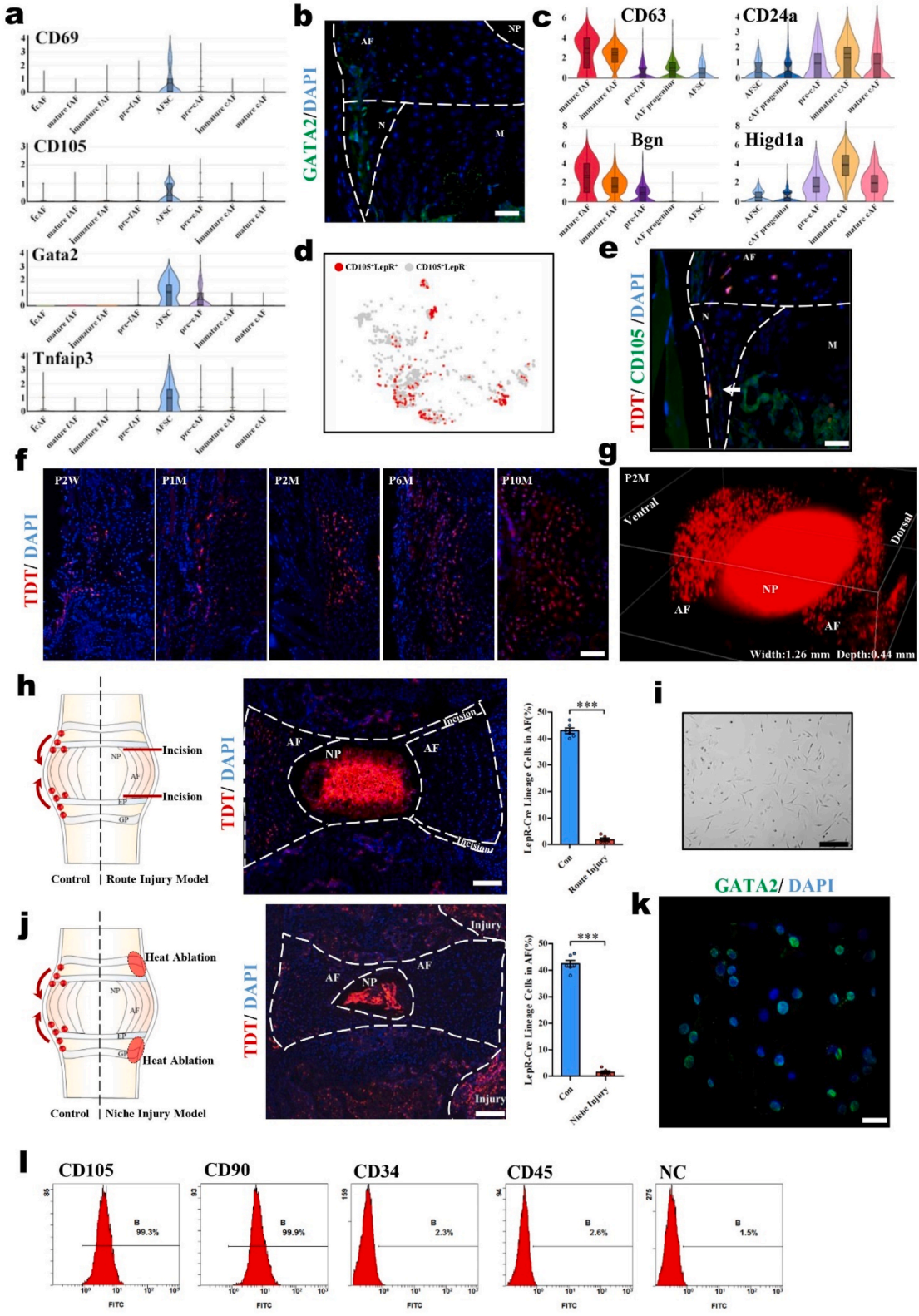

Fig. 2. AFSCs are appropriate seed cells for AF reconstruction with the abilities to migrate and differentiate. (a) Violin plots showing the expression levels of stem cell markers for AF populations. (b) Immunofluorescence staining of GATA2 in mouse IVDs (P2M). (c) Violin plots showing the expression levels of differentiation-related genes in AF populations. (d) Dot plots showing the LepR$^+$ cells in the CD105$^+$ cells on the t-SNE map. (e) Immunofluorescence staining of CD105 in the IVDs of LepR-cre; tdTomato mice (P2M). Scale bar, 50 μm. Arrowhead, colocalization of CD105 and tdTomato. M, metaphysis; N, niche. (f) Immunofluorescence images of LepR-cre; tdTomato mice of different ages. Scale bar, 100 μm. P, postnatal. W, weeks. M, months. (g) 3D reconstruction of the immunofluorescence images of lumbar IVDs in LepR-cre; tdTomato mice (P2M). Schematic diagrams, immunofluorescence images, and the tdTomato$^+$ cells statistical data of (h) the migratory route injury model and (j) the niche injury model of LepR-cre; tdTomato mice. Scale bar, 100 μm. (i) Cell morphology of cultured AFSCs. Scale bar, 50 μm. (k) Immunofluorescence staining of GATA2 in cultured AFSCs. Scale bar, 20 μm. (l) Flow cytometric analysis of CD105, CD90, CD34, and CD45 expression in cultured AFSCs (n = 6, $^{***}P <$ 0.001 vs. control group. For all the above-mentioned statistical analyses, significance was determined by student's-*t* tests and the results were shown as mean ± SD.).

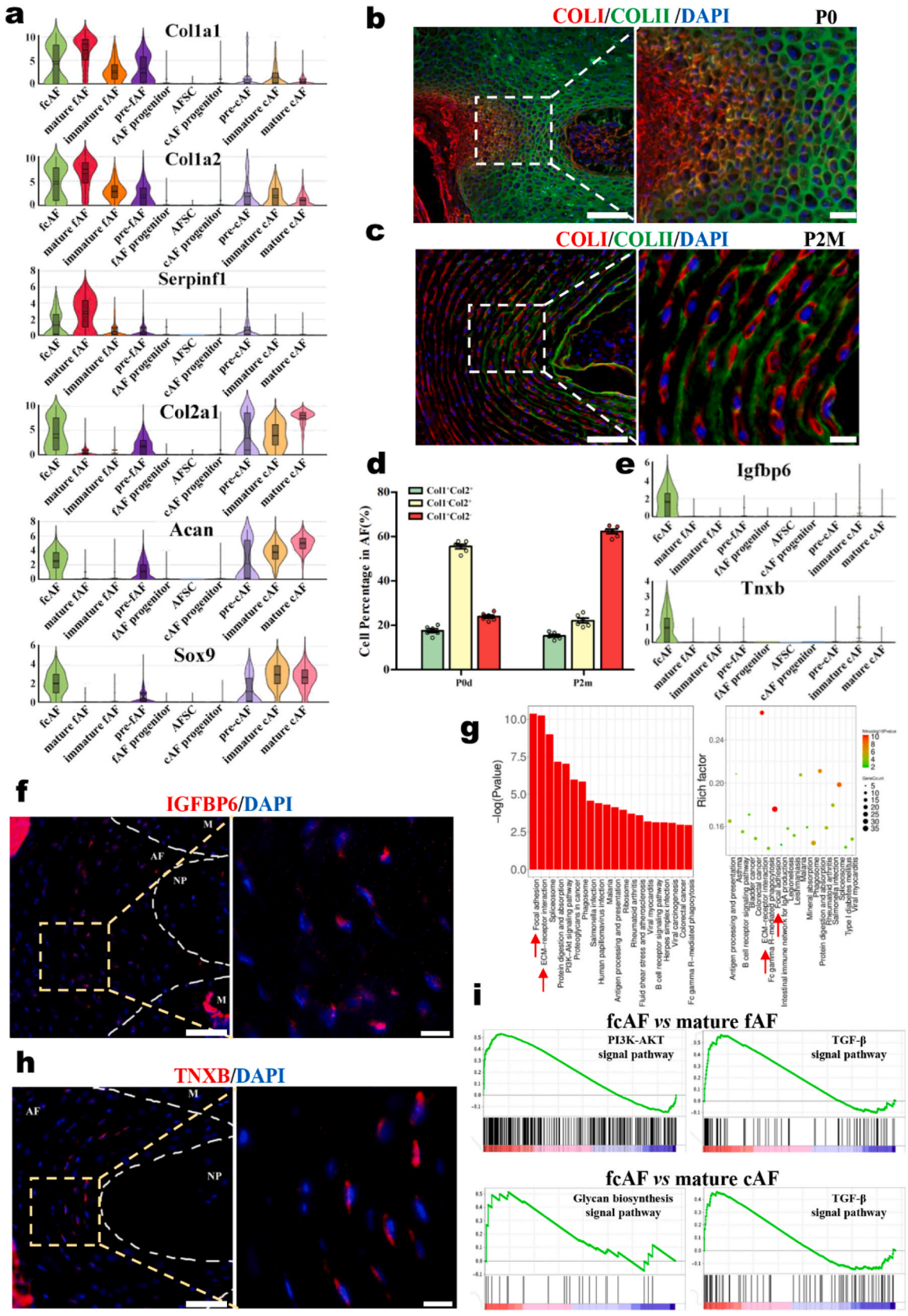

Fig. 3. The identity of a novel population of AF cells, fcAFs. (a) Violin plots showing the expression levels of classical oAF and iAF markers in AF populations. Immunofluorescence staining of COLI and COLII in the IVDs of (b) P0day and (c) P2M mice. Scale bars, 100 μm (left), 20 μm (right). (d) Violin plots showing the expression levels of representative fcAF markers. (e) Statistical data of AF $Col1^{+}Col2^{+}$ cells. Immunofluorescence staining of the specificity markers (f) IGFBP6 and (h) TNXB in the IVDs of P2M mice. Scale bars, 100 μm (left), 20 μm (right). (g) KEGG analysis of the DEGs showing the enriched signaling pathways in fcAFs. (i) Gene set enrichment analysis (GSEA) showing the enrichment of pathways between fcAFs and fAFs or between fcAFs and cAFs.

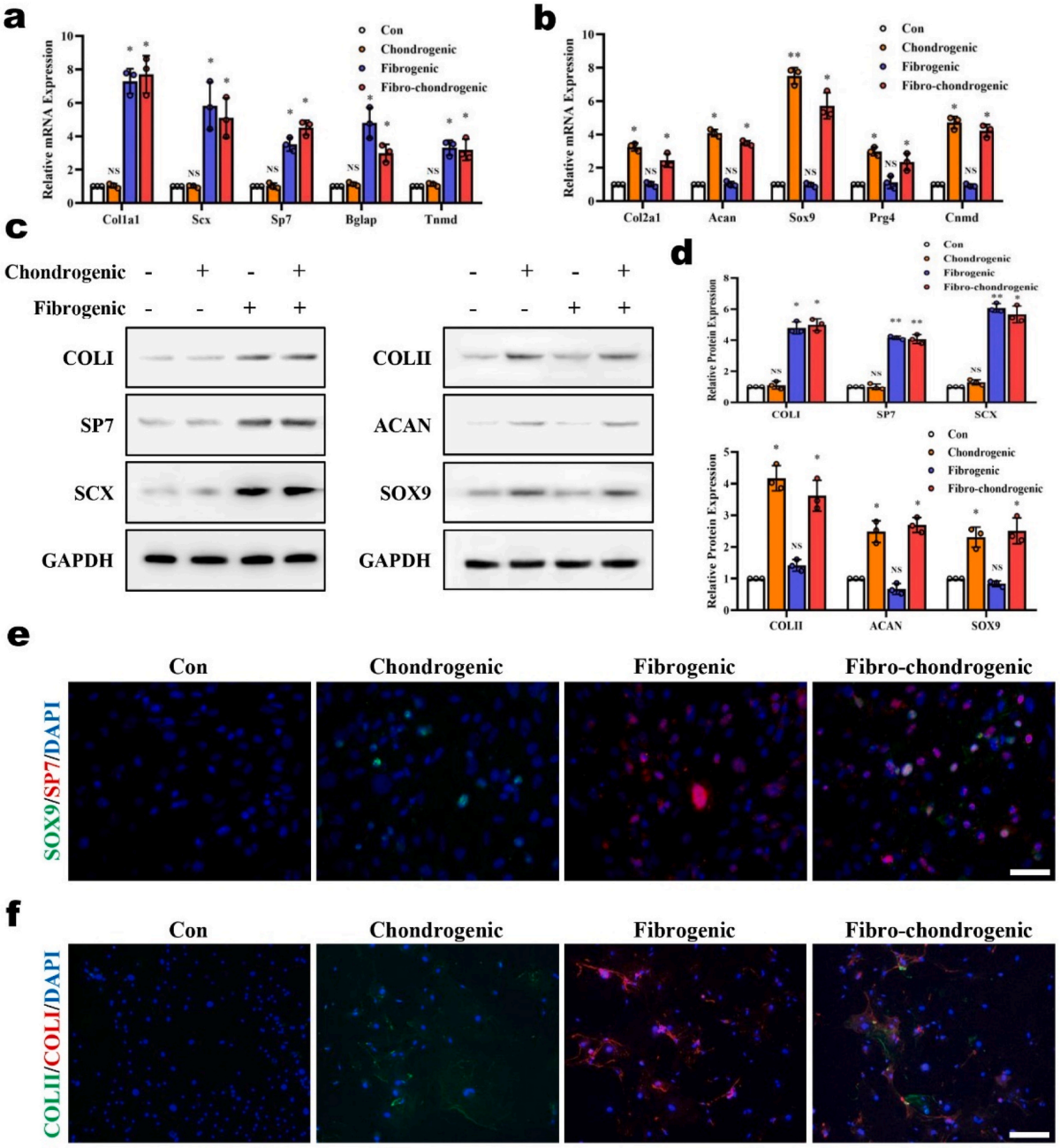

Fig. 4. Verification of the inductive effects of FCI on AFSCs *in vitro*. Real-time RT-PCR analysis of the expression of (a) fibrogenic markers and (b) chondrogenic markers in primary AFSCs after different inductions. (c) Western blot analysis of fibrogenic markers and chondrogenic markers in primary AFSCs after different inductions and (d) the corresponding statistical data. (e) Immunofluorescence staining of Sp7 and Sox9 in primary AFSCs after different inductions. Scale bar 50 μm. (f) Immunofluorescence staining of COLI and COLII in primary AFSCs after different inductions. Scale bar, 50 μm (n = 3, $^{*}P < 0.05$ vs. control group, $^{**}P < 0.01$ vs. control group, NS: not statistically significant vs. control group. For all the above-mentioned statistical analyses, significance was determined by one-way ANOVA followed by Dunnett's multiple comparisons test and the results were shown as mean ± SD.).

medium but not in fibrogenic medium (Fig. 4b). Similar results were observed at the protein level, and both fibrogenic and chondrogenic markers were simultaneously upregulated by fibrochondrogenic induction (Fig. 4c and d). Further dual-color immunostaining results showed that some AFSCs expressed both SP7 and Sox9 after FCI induction, indicating that these AFSCs were undergoing a differentiation process toward fcAFs (Fig. 4e). These cells synthesized and secreted both COLI and COLII (Fig. 4e and f) as extracellular matrix (Fig. 4f). Based on the above results, we successfully induced AFSCs to generate fcAFs *in vitro* by using the FCI. With the ability to simultaneously express and secrete COLI and COLII, fcAFs are the ideal target for induction during AF reconstruction.

3.5. SFMA/HAMA/FCI composite hydrogels could induce AFSC differentiation into fcAFs

Since AF tissue is composed of a fibrinoid matrix in the oAF and a chondroid matrix in the iAF, it is unbefitting to repair the full-thickness AF defects with a single biomaterial, as in most previous studies [39]. To match the structural and biomechanical characteristics of the two kinds of AF matrices, we chose silk fibroin (SF) and hyaluronic acid (HA) as the basal components of the composite hydrogel. SF is a natural, high

molecular weight fiber protein extracted from silk that has appropriate flexibility, tensile strength, moisture permeability and controlled release ability. Many studies have shown that SF hydrogels can stimulate MSCs to differentiate into fibroblasts or osteoblasts and were usually used to repair fibrous tissues such as tendons and bones [40–42]. In addition, HA is a high molecular weight polysaccharide composed of two disaccharide units, D-glucuronic acid and N-acetylglucosamine, which has high water retention, viscoelasticity, and biocompatibility. HA hydrogels can induce the differentiation of MSCs into chondrocytes and is usually used to repair articular cartilage [43–45]. Based on the above characteristics, we combined SF and HA to form composite hydrogels for AF repair. To optimize the curing process of the composite hydrogel, we methacrylated both SF and HA (SFMA and HAMA) to make the hydrogel photocurable [46]. To enhance the inductive capacity, FCI was also added to the composite hydrogel.

We prepared the SFMA/HAMA/FCI composite hydrogel, which was cured for 30–40 s under blue light (Fig. 5a). Fourier transform infrared (FTIR) analysis found that the characteristic peaks of SFMA were at 1644 cm^{-1} (amide I) and 1535 cm^{-1} (amide I), and the characteristic peaks of HAMA were found at 1602 cm^{-1} and 1030 cm^{-1}, which were consistent with those reported previously [47–49]. The characteristic peaks of SFMA/HAMA were mainly superposed by those from SFMA and HAMA. In addition, the 1743 cm^{-1} peak (ester bond) was enhanced in SFMA/HAMA, indicating that acylation or esterification could be strengthened by the hybrid reaction of SFMA and HAMA (Fig. 5b). Compared with SFMA/HAMA, the amide II peak at 1535 cm^{-1} gradually shifted to 1515 cm^{-1}, and the amide III absorption peak at 1235 cm^{-1} increased slightly in SFMA/HAMA/FCI, indicating that the number of β-sheets in the composite hydrogel had increased [50,51] (Fig. 5b and Supplementary Fig. 5). Furthermore, we performed ^{1}H-NMR to analyze the differences between SFMA/HAMA and SFMA/HAMA/FCI, and we found that the peaks at 3.6 ppm and 4.1 ppm were the characteristic peaks from β-glycerophosphate in SFMA/HAMA/FCI. Moreover, the relative abundance of the methacrylate structure (2.0 ppm) was 1.04 in SFMA/HAMA/FCI, which was 18.2% higher than that in the SFMA/HAMA spectrum, indicating that methacrylation was promoted and further contributed to the composite hydrogel light curation (Fig. 5c and Supplementary Fig. 6).

By scanning electron microscopy (SEM), we found that the composite hydrogel formed a relatively uniform void structure. The pore sizes of the composite hydrogels were between that of the SFMA hydrogel (68.4 ± 13.9 μm) and that of the HAMA hydrogel (152.3 ± 30.7 μm), and the difference in pore size between the SFMA/HAMA composite hydrogel (92.3 ± 17.9 μm) and SFMA/HAMA/FCI composite hydrogel (97.3 ± 15.1 μm) was not significant (Fig. 5d, f). Further energy spectral analysis showed that the SFMA/HAMA/FCI composite hydrogel had increased phosphorus and sodium contents compared with the SFMA, HAMA and SFMA/HAMA composite hydrogels (Fig. 5e). In addition, the mechanical test results showed that the mechanical properties of the SFMA/HAMA composite hydrogel were between those of the SFMA hydrogel and HAMA hydrogel, and the compression modulus of the SFMA/HAMA/FCI composite hydrogel was higher than that of the SFMA/HAMA composite hydrogel (Fig. 5g and h), which is indicative of changes in the molecular structure of the composite hydrogel caused by the mixing with FCI. Further testing of drug release from the light-cured hydrogel showed that FCI mixing improved the controlled release ability from the composite hydrogel and prolonged the release period of TGF-β3 and β-GP (Fig. 5i and Supplementary Fig. 7). Further cell loading experiments showed that these four kinds of hydrogels were biocompatible, and AFSCs grew uniformly in each of them (Fig. 5j). Further qRT-PCR analysis showed that the SFMA/HAMA/FCI composite hydrogel significantly upregulated the mRNA levels of the fibrogenic markers Col1a1, Scx, Sp7, Bglap and Tnmd. Moreover, the mRNA levels of the chondrogenic markers Col2a1, Acan, Sox9, Prg4 and Cnmd were significantly upregulated in the SFMA/HAMA/FCI composite hydrogel (Fig. 5k and l).

In summary, we developed a novel composite hydrogel that could induce AFSC differentiation into fcAFs and found that it was promising for AF reconstruction.

3.6. AFSC-laden SFMA/HAMA/FCI composite hydrogels showed significant therapeutic efficacy after AF injury

We found that the SFMA/HAMA/FCI composite hydrogel had bright application prospects for AF reconstruction from the *in vitro* experiments, so we further tested the effects of this composite hydrogel on the reconstruction of AF defects *in vivo*. A box-shaped defect was established on mouse coccygeal IVDs, and then the AFSC-laden SFMA/HAMA/FCI composite hydrogel was dropped into the AF defect region followed by curing with blue light irradiation (Fig. 6a). First, we used tdTomato-labeled AFSCs to verify the survival of the implanted cells, and we found that most of the implanted cells survived for 3 weeks post-transplantation (Fig. 6b). Moreover, by examining the fluorescence intensity, the composite hydrogels were proven to be relatively stable after subcutaneous implantation for 4 weeks (Supplementary Fig. 8).

Two months after AF modeling and defect reconstruction, the samples were collected to detect the effects of the hydrogel on AF reconstruction. Safranin O/Fast Green staining showed that, in the baseline (BL) and control (Con) groups, the AF lamellae were highly aligned and the Safranin O stains were more than 60% of AF aera. In the AF injured group, the AF lamellae were replaced by fibrous scars that were arranged in a disorderly manner, and distance between bilateral growth plates was significant decreased (Supplementary Fig. 9). In the SFMA/HAMA and AFSC-laden SFMA/HAMA group, the AF lamellae had partially recovered, but no more than 10% of AF aera was stained by Safranin O dye, suggesting that the chondroid matrix of the iAF had barely recovered. In the AFSC-laden SFMA/HAMA/FCI group, in addition to the recovery of AF lamellae, 31.68% of AF aera was stained by Safranin O dye which was significantly more intense than that in the other hydrogel groups, indicating that the chondroid matrix was partially restored (Fig. 6c, e). Further quantitative histological assessments showed that the AF histological scores of the AF injured group, SFMA/HAMA group, and AFSC-laden SFMA/HAMA groups were significantly higher than those of the Con group, while the score of the AFSC-laden SFMA/HAMA/FCI group had partially retreated (Fig. 6d).

To observe the microstructure of the repaired areas, we conducted SEM examinations and found that the AF lamellae of the AF injured group, SFMA/HAMA group, and AFSCS-laden SFMA/HAMA group were disordered and that cracks remained in the repaired areas. However, the AF lamellae were partially re-established in the AFSC-laden SFMA/HAMA/FCI group. Moreover, the repaired area was tightly integrated with the original fibers without the appearance of any cracks (Fig. 6f). In addition, immunofluorescence tests showed that the main matrix of the repaired AF area was COLI, and COLII was hardly detectable in the AF injured group, SFMA/HAMA group, and AFSC-laden SFMA/HAMA groups. However, in the AFSC-laden SFMA/HAMA/FCI group, there was more COLII staining in the inner part of the repaired area (Fig. 6g), and the number of COLII-positive cells was significantly greater than that in the other groups (Fig. 6h). In addition, there were some areas in which COLI and COLII had colocalized. suggesting that fcAFs were successfully induced in the AFSC-laden SFMA/HAMA/FCI group (Fig. 6g). Based on the above results, we verified that the AFSC-laden SFMA/HAMA/FCI hydrogels were more effective during AF reconstruction because of their capacity to recover the chondroid matrix.

4. Discussion

Millions of people are suffering from low back pain and nerve irritation caused by IVDD, which significantly reduces quality of life and shortened life expectancy. The lack of repairing strategy of AF defects is held accountable to the poor treatment approaches of IVDD, largely. In this study, a deeper insight to the nature of AF was obtained by using the

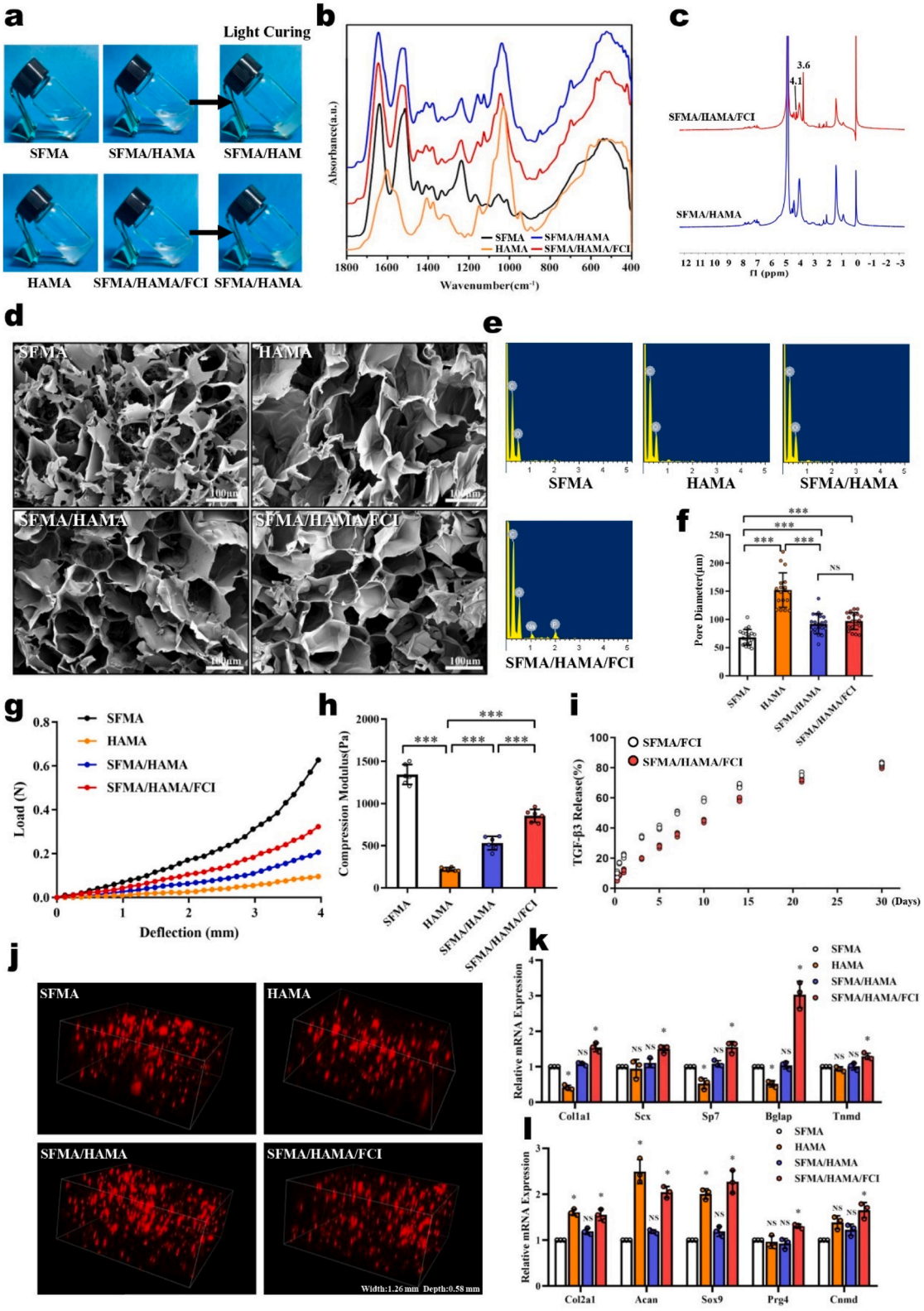

Fig. 5. The characterization and inductive effects of the SFMA/HAMA/FCI composite hydrogel. (a) Gross view of the composite hydrogels. (b) FTIR spectra of the composite hydrogels. (c) ^{1}H-NMR spectra of SFMA/HAMA and SFMA/HAMA/FCI. (d) Representative SEM images of the composite hydrogels. Scale bars, 100 μm. (e) Energy spectrum analysis of the composite hydrogels. (f) Bore diameters statistics of the composite hydrogels. (g) Load-deflection curves of the composite hydrogels. (h) Compression modulus of the composite hydrogels. (i) Drug release curves of the SFMA/HAMA and SFMA/HAMA/FCI composite hydrogels. (j) 3D reconstruction immunofluorescence images of tdTomato-labeled AFSCs cultured in the composite hydrogels. Real-time RT-PCR analysis of the expression of (k) fibrogenic markers and (l) chondrogenic markers in AFSCs cultured in the composite hydrogels (n = 3, $^{*}P < 0.05$ vs. SFMA group, $^{**}P < 0.01$ vs. SFMA group, $^{***}P < 0.01$ vs. SFMA group, NS: not statistically significant vs. SFMA group. For all the above-mentioned statistical analyses, significance was determined by one-way ANOVA followed by Dunnett's multiple comparisons test and the results were shown as mean ± SD.).

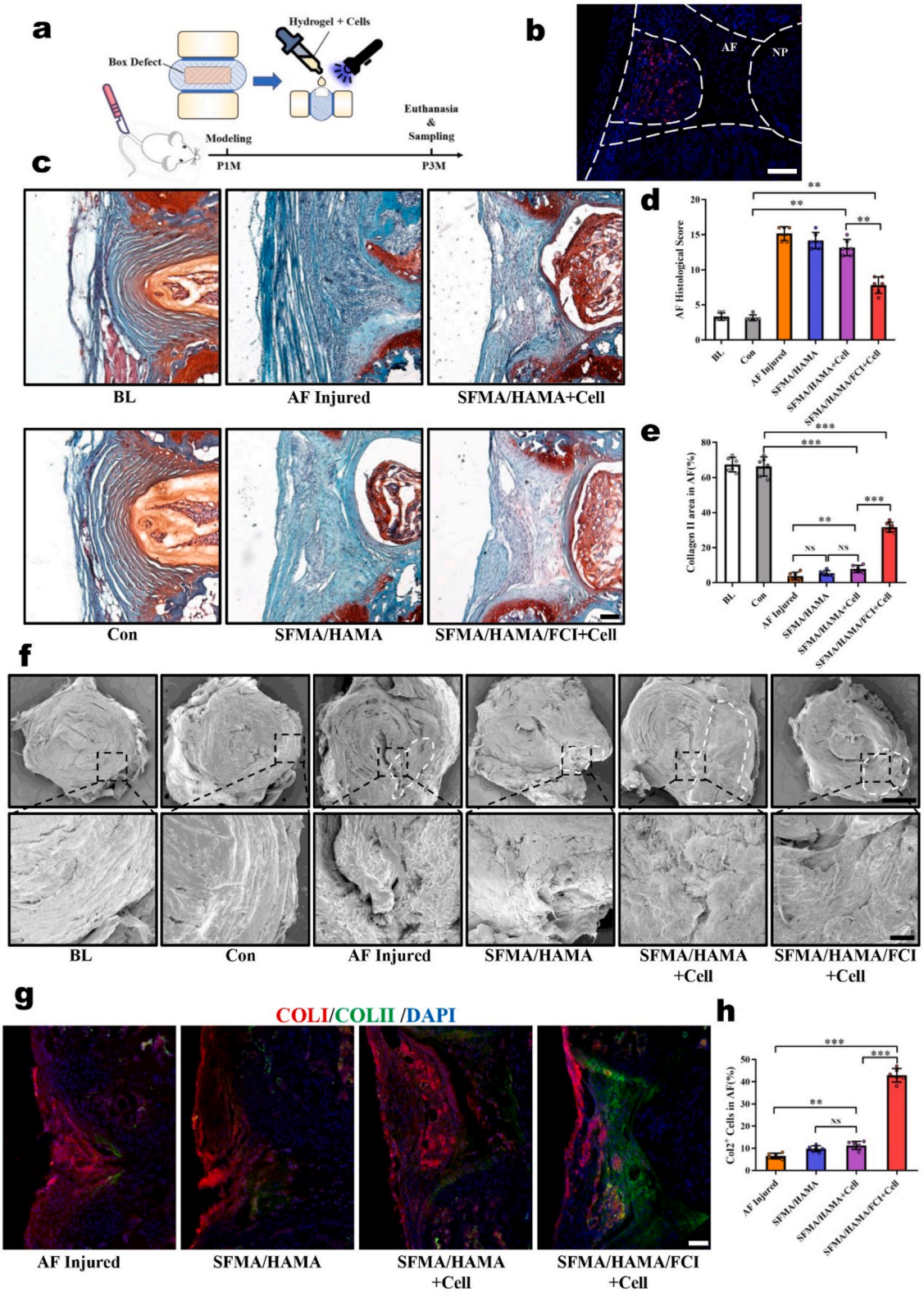

Fig. 6. Evaluation of repair efficacy in a mouse AF defect model. (a) Schematic diagram illustrating the experimental design. (b) Immunofluorescence image of the AF defects repaired by tdTomato-labeled AFSCs for 3 weeks. Scale bar, 50 μm. (c) Safranin O/Fast Green Staining of AF defects repaired by the composite hydrogels for 2 months. Scale bar, 100 μm. (d) The AF histological scores and (e) COLII areas in different groups. (f) Representative SEM images of AF defects repaired by the composite hydrogels for 2 months. Scale bars, 500 μm (top), 100 μm (bottom). (g) Immunofluorescence staining of COLI and COLII in the AF defects repaired by the composite hydrogels for 2 months. Scale bar, 100 μm. (h) The statistics of the number of $Col2^+$ cells in the AF-repaired areas in different groups. (n = 6, $^*P < 0.05$, $^{**}P < 0.01$, $^{***}P < 0.01$, NS: not statistically significant. Statistical analyses of COLII areas and $Col2^+$ cells used one-way ANOVA followed by Dunnett's multiple comparisons test; statistical analyses of AF histological scores used Kruskal-Wallis h-test followed by Dunn's multiple comparisons tests, and the results were shown as mean ± SD.)

scRNA-Seq, and an atlas of AF cells was decoded, based on which a novel and translation-promising strategy for AF reconstruction was proposed.

Unlike tendons or cartilages, which show a uniform matrix composition, AF matrix is composed of fibrinoid and chondroid matrices. This dual feature makes AF reconstruction a complex challenge. To solve this problem, identifying the cell composition contributed to this unique feature is the priority. Previous study reported that the AF cells can be roughly divided into three main categories, based on their anatomy location: inner AF cells, outer AF cells and other small populations, such as peripheral cells and interlamellar cells [22], and found the gene expression profiles of these populations were different from each other [52–55]. Such classification is quite simple and may mask the deeper physiological functions and connections between tissues and cells. Recently, Several subgroups of AF and NP were further revealed by scRNA-Seq [56–59]. However, the biological function and significance of AF subgroups still need to be further discovered. In our study, we detected and analyzed the AF cells by scRNA-Seq, identified the cell populations in histology, and proposed a naming system of AF cell populations by their biological functions and differentiation states instead of anatomic locations.

To reconstruct the AF injury exploiting tissue engineering strategy, a detailed atlas of AF cells is urgently needed. Besides, as AFSCs are a suitable candidate for seed cells in AF reconstruction, thus, it is necessary to sufficiently understand the *in vivo* evolution process of AFSCs. As previous studies reported, AFSCs were isolated and identified *in vitro* [17] and labeled with BrdU *in vivo* [60,61]. However, more evidence is still needed to further reveal the normal physiological status of AFSCs and provide a basis for their further application in tissue engineering for AF reconstruction. In this study, together with sequencing data, lineage tracing and histological verification, more evidences regarding the differentiation and migration of AFSCs were emerged, which increased the understanding of AFSCs.

Meanwhile, a new population of AF cells, fcAFs, was identified, which were detected to be in the middle layers of AF. Previous studies have also indicated that the middle layers of AF are different from oAF or iAF at the aspects of magnetic resonance imaging [62] and biomechanics [63]. Taking these differences into consideration, fibrous scaffirstfolds with various fiber diameters and orientation were used to repair oAF, iAF, and middle layers of AF respectively [64]. In our study, the new cell population provides the cytological reason of the morphology and structure differences among middle layers of AF, oAF, and iAF. Besides, this newly identified cell population could produce the two main matrix of the AF tissue, which could be regarded as a potential functional cell in AF reconstruction. Despite the significant translation potential, the current study also showed a temporal and spatial sequence of AF cells' differentiation and migration, which helped us to put more insight into the fundamental nature of AF, in both development and maturation aspects. Altogether, the results of the current study unmask the vague and constricted vision of the AF cellular composition, based on which a novel repairing strategy of AF defects were put forward.

Previous attempt to repair AF defects exploiting single component is not satisfying, due to the dual feature of the AF. In a number of studies, the chondroid matrix was barely formed if the high-density collagen gel or fibrin gel were applied and the defect was mainly repaired by fibrosis tissue [12–14]. A recent study tried to solve this problem by heterogeneous electrospun fibrous scaffolds. The study demonstrated that AFSCs could be induced to fibrogenic or chondrogenic differentiation by changing the diameter and direction of fibrous scaffolds [64]. In this study, we selected SF and HA composite hydrogels to match the two matrix components, fibrinoid and chondroid matrices, of the AF, respectively. Besides, the inductive effect of this hydrogel was enhanced by the inductive supplement we developed, FCI, which could induce AFSCs differentiation into fcAFs to synthesize and secrete the exact two main AF matrices. After the implantation of this novel hydrogel, together with the interaction of surrounding tissue, a suitable microenvironment was provided for the proper AF reconstruction. And the differentiation of seed cells was under control in this repair microenvironment, and achieved better effect by improved the chondroid content during AF reconstruction.

Limitations of this study include that the work is based on murine, whose IVD may not be quite the same with human. Studies based on human samples are still needed to further verified the scRNA-seq data and evaluate the therapeutical effect of this AF reconstruction strategy. Also, since the lamellar structure woven by parallel fibers of AF could be perfectly reconstructed by 3D bioprinting, more attempts should be made to produce a lamellar-structuralized hydrogel 3D bioprinting to meet the specific mechanical property of the AF.

5. Conclusion

To summarize, the AF cell atlas were decoded by scRNA-Seq and based on such deeper understanding of the fundamental nature of the AF, a novel strategy for AF reconstruction was proposed. This strategy is superior to the previous documented ones in the following three aspects: a newly identified seed cells with dual differentiation ability, a combined scaffold materials perfectly matching the dual features of the AF matrix components, and a formulated inductive supplement controlling the differentiation of implanted cells. By this way, this study innovatively developed a novel bioactive material for AF reconstruction and advanced the development of AF repair technology.

CRediT authorship contribution statement

Liu Yang, **Zhuojing Luo** and **Han Wang** designed the experiments. **Han Wang**, **Di Wang** and **Beier Luo** conducted most of the experiments. **Dong Wang** and **Houruo Jia** helped with the synthesis of composite hydrogel. **Qiliang Shang**, **Jianxin Mao**, and **Chu Gao** helped with animal experiments. **Ye Peng** and **Junjie Du** helped with the histological evaluation. **Pandi Peng** and **Lu Gan** helped with the statistical analysis. **Han Wang** and **Beier Luo** outlined and wrote the paper. **Liu Yang** supervised the study.

Declaration of competing interest

The authors declare that they have no competing financial interests or personal relationships that could have appeared influence the work reported in the paper.

Acknowledgements

We thank the financial support of the following funds for our study: The State Key Program of National Natural Science Foundation of China (Grant nos. 81730065 to Z.L., 82130070 to L.Y.), Projects of International Cooperation and Exchanges ofNational Natural Science Foundation of China (Grant nos. 82020108019 to Z.L.).

Appendix A. Supplementary data

Supplementary data to this article can be found online at https://doi.org/10.1016/j.bioactmat.2022.01.040.

References

[1] N.N. Knezevic, K.D. Candido, J. Vlaeyen, J. Van Zundert, S.P. Cohen, Low back pain, Lancet 398 (2021) 78–92.
[2] A.J. Rahyussalim, M. Zufar, T. Kurniawati, Significance of the association between disc degeneration changes on imaging and low back pain: a review article, Asian Spine J 14 (2020) 245–257.
[3] E.J. Novais, et al., Long-term treatment with senolytic drugs Dasatinib and Quercetin ameliorates age-dependent intervertebral disc degeneration in mice, Nat. Commun. 12 (2021) 5213.
[4] K. Ito, L. Creemers, Mechanisms of intervertebral disk degeneration/injury and pain: a review, Global Spine J. 3 (2013) 145–152.

[5] E.S. Fuller, C. Shu, M.M. Smith, C.B. Little, J. Melrose, Hyaluronan oligosaccharides stimulate matrix metalloproteinase and anabolic gene expression in vitro by intervertebral disc cells and annular repair in vivo, J Tissue Eng Regen Med 12 (2018) e216–e226.

[6] A.H. Bateman, C. Balkovec, M.K. Akens, et al., Closure of the annulus fibrosus of the intervertebral disc using a novel suture application device-in vivo porcine and ex vivo biomechanical evaluation, Spine J. 16 (2016) 889–895.

[7] Z.Z. Li, Z. Cao, H.L. Zhao, W.L. Shang, S.X. Hou, A pilot study of full-endoscopic annulus fibrosus suture following lumbar discectomy: technique notes and one-year follow-up, Pain Physician 23 (2020) E497–E506.

[8] A. Bartlett, L. Wales, R. Houfburg, W.K. Durfee, S.L. Griffith, I. Bentley, Optimizing the effectiveness of a mechanical suture-based anulus fibrosus repair construct in an acute failure laboratory simulation, J. Spinal Disord. Tech. 26 (2013) 393–399.

[9] W.J. Choy, K. Phan, A.D. Diwan, C.S. Ong, R.J. Mobbs, Annular closure device for disc herniation: meta-analysis of clinical outcome and complications, BMC Muscoskel. Disord. 19 (2018) 290.

[10] P.D. Klassen, G. Lesage, L.E. Miller, et al., Reoperation after primary lumbar discectomy with or without implantation of a bone-anchored annular closure device: surgical strategies and clinical outcomes, World Neurosurg 130 (2019) e926–e932.

[11] J.C. Kienzler, P.D. Klassen, L.E. Miller, et al., Three-year results from a randomized trial of lumbar discectomy with annulus fibrosus occlusion in patients at high risk for reherniation, Acta Neurochir (Wien) 161 (2019) 1389–1396.

[12] Z. Zhou, S. Zeiter, T. Schmid, et al., Effect of the CCL5-releasing fibrin gel for intervertebral disc regeneration, Cartilage (2018), 1947603518764263.

[13] B. Pennicooke, I. Hussain, C. Berlin, et al., Annulus fibrosus repair using high-density collagen gel: an in vivo ovine model, Spine (Phila Pa 1976) 43 (2018) E208–E215.

[14] P. Grunert, B.H. Borde, K.D. Hudson, M.R. Macielak, L.J. Bonassar, R. Härtl, Annular repair using high-density collagen gel: a rat-tail in vivo model, Spine (Phila Pa 1976) 39 (2014) 198–206.

[15] L. Xin, C. Zhang, F. Zhong, S. Fan, W. Wang, Z. Wang, Minimal invasive annulotomy for induction of disc degeneration and implantation of poly (lactic-co-glycolic acid) (PLGA) plugs for annular repair in a rabbit model, Eur. J. Med. Res. 21 (2016) 7.

[16] A.A. Hegewald, F. Medved, D. Feng, et al., Enhancing tissue repair in annulus fibrosus defects of the intervertebral disc: analysis of a bio-integrative annulus implant in an in-vivo ovine model, J Tissue Eng Regen Med 9 (2015) 405–414.

[17] C. Liu, Q. Guo, J. Li, et al., Identification of rabbit annulus fibrosus-derived stem cells, PLoS One 9 (2014), e108239.

[18] C. Liu, Z. Jin, X. Ge, Y. Zhang, H. Xu, Decellularized annulus fibrosus matrix/chitosan hybrid hydrogels with basic fibroblast growth factor for annulus fibrosus tissue engineering, Tissue Eng Part A 25 (23–24) (2019) 1605–1613.

[19] I. Hussain, S.R. Sloan, C. Wipplinger, et al., Mesenchymal stem cell-seeded high-density collagen gel for annular repair: 6-week results from in vivo sheep models, Neurosurgery 85 (2019) E350–E359.

[20] D. Oehme, P. Ghosh, S. Shimmon, et al., Mesenchymal progenitor cells combined with pentosan polysulfate mediating disc regeneration at the time of microdiscectomy: a preliminary study in an ovine model, J. Neurosurg. Spine 20 (2014) 657–669.

[21] Y. Wang, X. Wang, J. Shang, et al., Repairing the ruptured annular fibrosus by using type I collagen combined with citric acid, EDC and NHS: an in vivo study, Eur. Spine J. 26 (2017) 884–893.

[22] O.M. Torre, V. Mroz, M.K. Bartelstein, A.H. Huang, J.C. Iatridis, Annulus fibrosus cell phenotypes in homeostasis and injury: implications for regenerative strategies, Ann. N. Y. Acad. Sci. 1442 (2019) 61–78.

[23] Y. Gao, X. Li, C. Zeng, et al., CD63+ cancer-associated fibroblasts confer tamoxifen resistance to breast cancer cells through exosomal miR-22, Adv. Sci. 7 (2020) 2002518.

[24] Q. Guo, P. Zhou, B. Li, Identification and characterizations of annulus fibrosus-derived stem cells, Methods Mol. Biol. 1842 (2018) 207–216.

[25] C. Deng, J. Yang, H. He, et al., 3D bio-printed biphasic scaffolds with dual modification of silk fibroin for the integrated repair of osteochondral defects, Biomater Sci 9 (2021) 4891–4903.

[26] B. Velasco-Rodriguez, T. Diaz-Vidal, L.C. Rosales-Rivera, et al., Hybrid methacrylated gelatin and hyaluronic acid hydrogel scaffolds. Preparation and systematic characterization for prospective tissue engineering applications, Int. J. Mol. Sci. 22 (2021).

[27] A. Bucciarelli, T. Muthukumar, J.S. Kim, et al., Preparation and statistical characterization of tunable porous sponge scaffolds using UV cross-linking of methacrylate-modified silk fibroin, ACS Biomater. Sci. Eng. 5 (2019) 6374–6388.

[28] B.O. Zhou, R. Yue, M.M. Murphy, J.G. Peyer, S.J. Morrison, Leptin-receptor-expressing mesenchymal stromal cells represent the main source of bone formed by adult bone marrow, Cell Stem Cell 15 (2014) 154–168.

[29] R. Yue, B.O. Zhou, I.S. Shimada, Z. Zhao, S.J. Morrison, Leptin receptor promotes adipogenesis and reduces osteogenesis by regulating mesenchymal stromal cells in adult bone marrow, Cell Stem Cell 18 (2016) 782–796.

[30] B. Gao, J. Yin, X. Xu, et al., Leptin receptor-expressing cells represent a distinct subpopulation of notochord-derived cells and are essential for disc homoeostasis, J Orthop Translat 21 (2020) 91–99.

[31] H. Wang, Y. Zhou, T.W. Chu, et al., Distinguishing characteristics of stem cells derived from different anatomical regions of human degenerated intervertebral discs, Eur. Spine J. 25 (2016) 2691–2704.

[32] C. Liu, C. Zhu, J. Li, P. Zhou, M. Chen, H. Yang, B. Li, The effect of the fibre orientation of electrospun scaffolds on the matrix production of rabbit annulus fibrosus-derived stem cells, Bone Res 3 (2015) 15012.

[33] H.E. Gruber, F.E. Riley, G.L. Hoelscher, J.A. Ingram, L. Bullock, E.N. Hanley Jr., Human annulus progenitor cells: analyses of this viable endogenous cell population, J. Orthop. Res. 34 (2016) 1351–1360.

[34] O.M. Torre, V. Mroz, A. Benitez, A.H. Huang, J.C. Iatridis, Neonatal annulus fibrosus regeneration occurs via recruitment and proliferation of Scleraxis-lineage cells, NPJ Regen Med 4 (2019) 23.

[35] D. Lin, P. Alberton, M. Delgado Caceres, C. Prein, H. Clausen-Schaumann, J. Dong, A. Aszodi, C. Shukunami, J.C. Iatridis, D. Docheva, Loss of tenomodulin expression is a risk factor for age-related intervertebral disc degeneration, Aging Cell 19 (2020), e13091.

[36] F. Zanata, L. Curley, E. Martin, A. Bowles, B.A. Bunnell, X. Wu, L.M. Ferreira, J. M. Gimble, Comparative analysis of human adipose-derived stromal/stem cells and dermal fibroblasts, Stem Cell. Dev. 30 (2021) 1171–1178.

[37] S. Abubacker, P. Premnath, A. Shonak, C. Leonard, S. Shah, Y. Zhu, G.D. Jay, T. A. Schmidt, S. Boyd, R. Krawetz, Absence of proteoglycan 4 (Prg4) leads to increased subchondral bone porosity which can Be mitigated through intra-articular injection of PRG4, J. Orthop. Res. 37 (2019) 2077–2088.

[38] S. Zhu, H. Qiu, S. Bennett, V. Kuek, V. Rosen, H. Xu, J. Xu, Chondromodulin-1 in health, osteoarthritis, cancer, and heart disease, Cell. Mol. Life Sci. 76 (22) (2019) 4493–4502.

[39] S. Molladavoodi, J. McMorran, D. Gregory, Mechanobiology of annulus fibrosus and nucleus pulposus cells in intervertebral discs, Cell Tissue Res. 379 (2020) 429–444.

[40] F. Bi, Z. Shi, A. Liu, P. Guo, S. Yan, Anterior cruciate ligament reconstruction in a rabbit model using silk-collagen scaffold and comparison with autograft, PLoS One 10 (2015), e0125900.

[41] W. Zhang, C. Ling, A. Zhang, et al., An all-silk-derived functional nanosphere matrix for sequential biomolecule delivery and in situ osteochondral regeneration, Bioact Mater 5 (2020) 832–843.

[42] X. Wu, M. Zhou, F. Jiang, S. Yin, S. Lin, G. Yang, Y. Lu, W. Zhang, X. Jiang, Marginal sealing around integral bilayer scaffolds for repairing osteochondral defects based on photocurable silk hydrogels, Bioact Mater 6 (2021) 3976–3986.

[43] B. Teng, S. Zhang, J. Pan, et al., A chondrogenesis induction system based on a functionalized hyaluronic acid hydrogel sequentially promoting hMSC proliferation, condensation, differentiation, and matrix deposition, Acta Biomater. 122 (2021) 145–159.

[44] Y. Deng, G. Lei, Z. Lin, Y. Yang, H. Lin, R.S. Tuan, Engineering hyaline cartilage from mesenchymal stem cells with low hypertrophy potential via modulation of culture conditions and Wnt/β-catenin pathway, Biomaterials 192 (2019) 569–578.

[45] J. Chen, J. Yang, L. Wang, X. Zhang, B.C. Heng, D.A. Wang, Z. Ge, Modified hyaluronic acid hydrogels with chemical groups that facilitate adhesion to host tissues enhance cartilage regeneration, Bioact Mater 6 (2021) 1689–1698.

[46] Y. Wu, L. Wang, B. Guo, X. Ma, P, Injectable biodegradable hydrogels and microgels based on methacrylated poly(ethylene glycol)-co-poly(glycerol sebacate) multi-block copolymers: synthesis, characterization, and cell encapsulation, J. Mater. Chem. B 2 (2014) 3674–3685.

[47] S. Yan, Q. Wang, Z. Tariq, et al., Facile preparation of bioactive silk fibroin/hyaluronic acid hydrogels, Int. J. Biol. Macromol. 118 (Pt A) (2018) 775–782.

[48] L.M. Yu, T. Liu, Y.L. Ma, F. Zhang, Y.C. Huang, Z.H. Fan, Fabrication of silk-hyaluronan composite as a potential scaffold for tissue repair, Front. Bioeng. Biotechnol. 8 (2020) 578988.

[49] A. Pistone, A. Sagnella, C. Chieco, et al., Silk fibroin film from golden-yellow Bombyx mori is a biocomposite that contains lutein and promotes axonal growth of primary neurons, Biopolymers 105 (2016) 287–299.

[50] T. Zhong, C. Deng, Y. Gao, M. Chen, B. Zuo, Studies of in situ-forming hydrogels by blending PLA-PEG-PLA copolymer with silk fibroin solution, J. Biomed. Mater. Res. 100 (2012) 1983–1989.

[51] H. Li, J. Zhang, S. Liu, Y. Yan, X. Li, Consecutive dephosphorylation by alkaline phosphatase-directed in situ formation of porous hydrogels of SF with nanocrystalline calcium phosphate ceramics for bone regeneration, J. Mater. Chem. B 8 (2020) 9043–9051.

[52] J. Wang, Y. Huang, L. Huang, et al., Novel biomarkers of intervertebral disc cells and evidence of stem cells in the intervertebral disc, Osteoarthritis Cartilage 29 (2021) 389–401.

[53] K. Li, D. Kapper, B. Youngs, V. Kocsis, S. Mondal, P. Kraus, T. Lufkin, Potential biomarkers of the mature intervertebral disc identified at the single cell level, J. Anat. 234 (1) (2019) 16–32.

[54] P. Kraus, T. Lufkin, Bovine annulus fibrosus cell lines isolated from intervertebral discs, Genom Data 10 (2016) 83–84.

[55] C.R. Lee, D. Sakai, T. Nakai, K. Toyama, J. Mochida, M. Alini, S. Grad, A phenotypic comparison of intervertebral disc and articular cartilage cells in the rat, Eur. Spine J. 16 (12) (2007) 2174–2185.

[56] C.J. Panebianco, A. Dave, D. Charytonowicz, R. Sebra, J.C. Iatridis, Single-cell RNA-sequencing atlas of bovine caudal intervertebral discs: discovery of heterogeneous cell populations with distinct roles in homeostasis, Faseb. J. 35 (11) (2021), e21919.

[57] Y. Gan, J. He, J. Zhu, Z. Xu, Z. Wang, J. Yan, O. Hu, Z. Bai, L. Chen, Y. Xie, M. Jin, S. Huang, B. Liu, P. Liu, Spatially defined single-cell transcriptional profiling characterizes diverse chondrocyte subtypes and nucleus pulposus progenitors in human intervertebral discs, Bone Res 9 (2021) 37.

[58] M. Calió, B. Gantenbein, M. Egli, L. Poveda, F. Ille, The cellular composition of bovine coccygeal intervertebral discs: a comprehensive single-cell RNAseq analysis, Int. J. Mol. Sci. 22 (2021) 9.

[59] L.M. Fernandes, N.M. Khan, C.M. Trochez, M. Duan, M.E. Diaz-Hernandez, S. M. Presciutti, G. Gibson, H. Drissi, Single-cell RNA-seq identifies unique

transcriptional landscapes of human nucleus pulposus and annulus fibrosus cells, Sci. Rep. 10 (2020) 15263.
[60] H. Henriksson, M. Thornemo, C. Karlsson, et al., Identification of cell proliferation zones, progenitor cells and a potential stem cell niche in the intervertebral disc region: a study in four species, Spine (Phila Pa 1976) 34 (2009) 2278–2287.
[61] H.B. Henriksson, E. Svala, E. Skioldebrand, A. Lindahl, H. Brisby, Support of concept that migrating progenitor cells from stem cell niches contribute to normal regeneration of the adult mammal intervertebral disc: a descriptive study in the New Zealand white rabbit, Spine (Phila Pa 1976) 37 (2012) 722–732.
[62] Z. Shan, S. Li, J. Liu, M. Mamuti, C. Wang, F. Zhao, Correlation between biomechanical properties of the annulus fibrosus and magnetic resonance imaging (MRI) findings, Eur. Spine J. 24 (2015) 1909–1916.
[63] J. Li, C. Liu, Q. Guo, H. Yang, B. Li, Regional variations in the cellular, biochemical, and biomechanical characteristics of rabbit annulus fibrosus, PLoS One 9 (2014), e91799.
[64] P. Zhou, G. Chu, Z. Yuan, H. Wang, W. Zhang, Y. Mao, X. Zhu, W. Chen, H. Yang, B. Li, Regulation of differentiation of annulus fibrosus-derived stem cells using heterogeneous electrospun fibrous scaffolds, J Orthop Translat 26 (2021) 171–180.